# Microstructures and Phases Analysis of the 60Al-40V Master Alloy Produced by the Aluminothermic Process

Tresor O. Mapoli[1,*], Kalenda Mutombo[2], Kofi A. Annan[1] & Charles W. Siyasiya [1]

[1]Department of Materials Science and Metallurgical Engineering, University of Pretoria, Lynnwood Road, Hatfield, 0028, Pretoria, South Africa

[2]Light Metals, Materials Science & Manufacturing, Council for Science and Industrial Research, Meiring Naude Road, Brummeria, 0185, Pretoria, South Africa

*Correspondence to Tresor O. Mapoli. Email: u12281248@tuks.co.za

## Abstract

Aluminothermic reaction process was used to produce the 60Al-40V master alloy from pure Al metal and vanadium pentoxide ($V_2O_5$). Material characterization techniques including light optical microscopy (LOM), scanning electron microscopy (SEM), energy-dispersive X-ray spectroscopy (EDS), and X-ray diffraction (XRD) were employed to analyse the microstructural, chemical composition and phases present in the alloy. Thermal analysis was carried out on the alloy using simultaneous differential scanning calorimetry and thermogravimetry (DSC-TG) analysis to determine the phase transformations. The microstructural analysis through both LOM and SEM indicated that the starting material consisted of the columnar dendritic structure. After the double heating cycle during the DSC-TG tests, the dendrite structure transformed to the globular structure. The globularization was attributed to the dendrite fragmentation obtained when heating the as-cast materials in the solid-liquid region. This globular shape playing a positive role in enhancing the properties of the alloy. Through DSC-TG analysis, different peaks of transition temperatures were detected showing that the phase transformations occurred during the heating and cooling processes. The Al-rich phase ($Al_{21}V_2$) did not dissolve during homogenization. However, the intermetallic $Al_8V_5$ phase transformed to the $Al_3V$ phase during cooling. The chemical analysis of the produced master alloy was found to be 63 Al and 37 wt. % V. The phases in the alloy were principally identified to be $Al_3V$ and $Al_8V_5$ intermetallic phases. The analysis of the results shows that the most stable phase found at high temperature was the $Al_3V$ phase.

**Keywords:** Microstructures; Phases; Aluminothermy; Temperature; Composition

## Introduction

Ti-based alloys have gained significant attention in the aerospace, automotive and medical industries due to their excellent properties such as low weight, high strength, high toughness, and good property retention at elevated temperatures [1, 2]. The most commonly used Ti-based alloy is the Ti-6Al-4V which is widely used in many applications [3,4,5,6,7,8]. The blended elemental (BE) and the pre-alloyed (PA) approaches are the most widely used powder

metallurgy (PM) methods employed in the production of the Ti-6Al-4V [9]. In the latter method, the pre-alloyed 60Al-40V master alloy which is a semi-finished product is commonly used in the development of the Ti-6Al-4V alloy [10]. The methods used to produce Al-based master alloys include mixing processes [11,12,13], sintering and mechanical alloying methods [14]. However, the high cost of the alloying elements and high material loss during the alloying process are the main disadvantages of these processes [15]. The two-step process, namely the aluminothermic-vacuum melting method, allows obtaining highly pure, homogeneous Al-based master alloys with the lowest possible content of impurities [16]. However, this process is complicated, and the cost involved is also high [17]. Therefore, the aluminothermic reaction process has been considered as an effective technique for the production of the Al-based master alloys [18,19,20] with reduced production costs. In more recent times, Al-V master alloy has been produced through the aluminothermic reaction process using either $V_2O_5$ or $V_2O_3$ and pure Al metal [20]. In the aluminothermic reaction process, Al metal and vanadium pentoxide ($V_2O_5$) are mixed in the Al: $V_2O_5$ weight ratio from 0.25 to 0.75 [21], resulting in an exothermic reaction capable of producing the Al-V alloys [22]. The $V_2O_5$ and Al powders are used as the starting material in the aluminothermic reaction to produce Al-V alloys, and the two elements are mixed to produce a reaction as described in Eq 1:

$$3V_2O_5 + 16\ Al \rightarrow 6\ AlV + 5\ Al_2O_3 + heat \quad (1)$$

The targeted alloy in the process described in Eq 1 is the production of a 60 Al and 40 wt. % V master alloy with intermetallic phases. The intermetallic phase alloys have attracted a lot of research interest due to their low density, high strength, resistance against corrosion and oxidation [17, 23,24,25,26]. Due to the high demand for high-quality titanium alloys, Al-V alloys of high homogeneous composition with high quality in terms of thermal conductivity, hardness and lowest content of impurities have received considerable attention [17, 24,25,26,27]. The complicated process involved in the reduction and oxidation of elements leads to the production of different phases and less homogeneity in the alloy [22]. It is, therefore, necessary to study the homogeneity of the aluminothermy produced alloy by characterizing the phases and the microstructures formed to understand and optimize the process in order to improve the quality of the alloy. This study combined different techniques ranging from light optical microscopy, scanning electron microscopy, and X-ray diffraction to thermal analysis to study the microstructures and the phases formed in the 60Al-40V master alloy produced through the aluminothermic process.

## Experimental Materials and Procedure

### *Materials*

Commercially produced vanadium pentoxide ($V_2O_5$) particles with a diameter between 7 and 20 mm and 99 % purity aluminium (Al) with particles of diameter between 1 and 3 mm and CaO powder of $\leq 50$ μm, as by suppliers, were used in the current study.

### *Experimental Procedure*

Pure Al metal (99 % purity) and $V_2O_5$ were mixed in a ratio of 1:2 (Al: $V_2O_5$) and then placed in a crucible. The CaO as an additive was used to flux the alumina forming during the reduction of vanadium oxide. High-purity electrodes were used to ignite the mixture in the furnace. The measured furnace temperature reached 1900 °C due to the exothermic nature of the reaction which made the melting of the starting elements to form the Al-V alloy. The electrode voltage

was ensured to be at 1.1kV while the material was continuously charged in the furnace. On completion of the reduction, the furnace was allowed to cool for 72 hours. The slag was observed to be separated from the alloy on cooling.

### *Material Characterization*

The compositions of the materials were analysed by inductively coupled plasma mass spectrometry (ICP). The phase evolution was traced using a PANalytical X'Pert pro powder diffractometer equipped with the X'Celerator detector and Co-Kα radiation (λ=1.789A). The phase constitution was determined by the XRD analysis. The crystal structure was determined by the selection of the best-fitted patterns from the International Centre for Diffraction Data (ICCD) database. The X'Pert High Score Plus software was used to measure the diffraction patterns and determine the relative phase amounts (weight % of the crystalline) using the Rietveld method (X'Pert High score plus).

The samples were prepared for image analysis following metallographic techniques according to the ASTM standard E3-11 [27] which included the mounting of samples, grinding using P400-P1200 SiC abrasive papers, fine polishing up to 0.25 μm and finished with an OP-S suspension and etched with diluted Kroll's reagent. The microstructures of the samples were characterized by light optical microscopy (LOM) and scanning electron microscopy (SEM) techniques. The chemical composition of the phases was determined using SEM coupled with an AZtec X-Max energy-dispersive X-ray spectroscopy (EDS) by carrying out line scans of specific microstructure with an oxford instrument Si (Li) X-ray detector incorporated in a Jeol JSM 7500F equipment operating at 15 kV. The thermal analysis, using simultaneous differential scanning calorimetry and thermogravimetry (DSC-TG) analysis, was carried out in a calibrated DSC-TG apparatus SDT Q600 V20.9 under an argon-controlled atmosphere. The specimens for the DSC-TG tests were quite small and irregular in shape and therefore were simply weighed. In other words, the masses were 11.48, 11.06, and 55.70 mg. In the DSC-TG analysis, three sets of experiments performed were characterized by the heating of samples from room temperature to the estimated temperatures of 1100, 1300 and 1400 °C, respectively, followed by furnace cooling to room temperature in two successive cycles. In other words, the samples were placed in an $Al_2O_3$ crucible and heated from room temperature to the above-mentioned temperatures then cooled to room temperature, reheated, and cooled similarly in a second cycle. The heating rate was maintained at 20 °C/min.

## Results and Discussion

### *Theoretical Predictions*

The Thermo-Calc$^{TM}$ software was used to study the phases present at given compositions and conditions of interest to the study. The Thermo-Calc$^{TM}$ predictions showed that the predominant phases in the Al-V system at the compositions range of ~60 Al–40 wt. %V at the temperatures considered in this study are $Al_8V_5$, $Al_3V$, and $Al_{23}V_4$. The full details of the Thermo-Calc$^{TM}$ predictions including the images are discussed elsewhere [28]. The predictions showed that the volume fraction of the $Al_8V_5$ phase appears to be decreasing with decreasing V content. The $Al_8V_5$ which has been reported to be a brittle phase was predicted to disappear with decreasing temperature [17]. On the other hand, the $Al_3V$ seems to become more pronounced with decreasing temperature and V content.

### *Chemical Composition*

Table 1 presents the results of the inductively coupled plasma mass spectrometry (ICP) analysis of the aluminothermy produced alloy.

**Table 1.** Elemental composition of the alloy produced in wt. %

| Elements | Al | V | Si | Fe | Cu | Ti | Sn | Pb |
|---|---|---|---|---|---|---|---|---|
| Sample 1 | 62.9 | 36.1 | 0.31 | 0.17 | 0.02 | 0.05 | 0.01 | 0.07 |
| Sample 2 | 64.9 | 33.2 | 0.09 | 0.23 | 0.14 | 0.05 | 0.01 | 0.07 |

The average compositions of the Al and V in the alloy based on the analysis were calculated to be 63.9 and 34.7, respectively. This result shows that the composition of the aluminothermy produced alloy is pretty much comparable to the theoretical 60Al-40V master alloy.

### *Microstructural Analysis and Elemental Composition*

Figure 1a shows the optical micrograph of the aluminothermy produced 60Al-40V master alloy in the as-cast conditions which exhibited columnar dendritic structure. The solidified microstructure consists of large primary dendrite and secondary dendrite grains forming on both sides of the primary dendrite grains. Figure 1b shows the morphology of the alloy after the DSC-TG test. It can be observed that the dendrite microstructure did not dissolve completely after the two-heating cycle during the DSC-TG test but simply globularized. Similar morphology of the dendrite structures was observed under the SEM, in Fig. 2. As may also be seen, the dendritic structure was not only retained but the phase distribution remained homogeneous before and after heat treatment through the DSC-TG double heating tests.

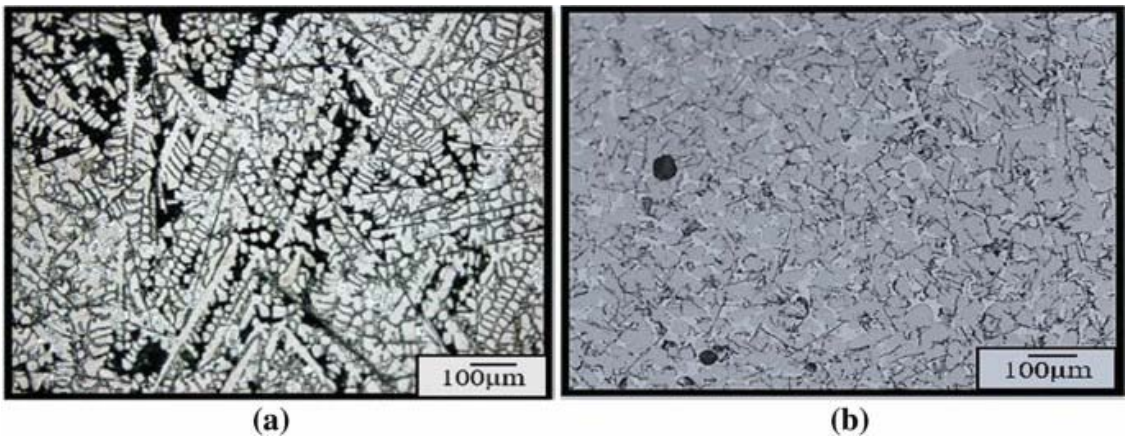


**Fig. 1.** Optical micrographs (**a**) in as-cast conditions, and (**b**) after DSC-TG double heating test at 1300 °C

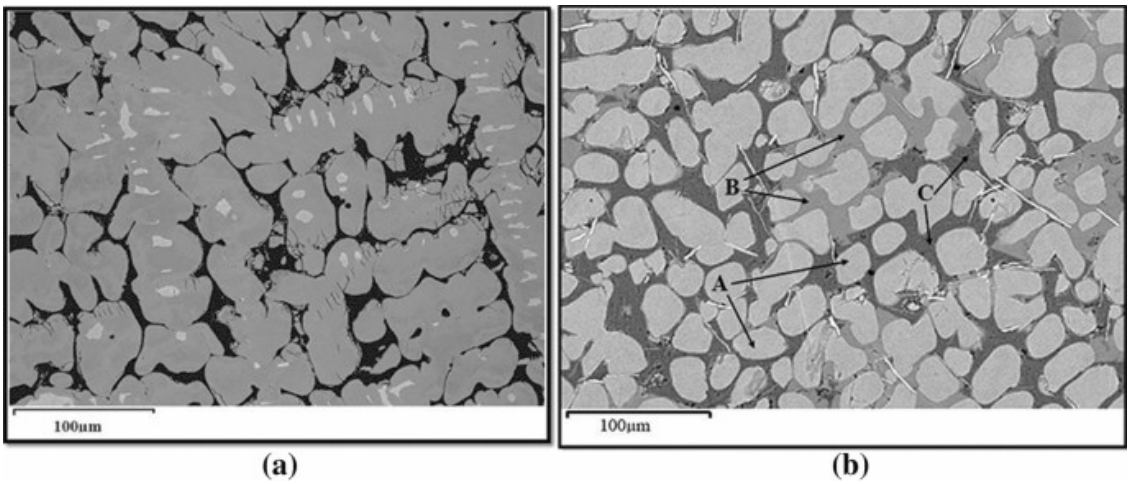


**Fig. 2.** The SEM micrographs (**a**) in as-cast conditions, (**b**) after the DSC-TG test at 1300 °C

In Figs. 1 and 2, the microstructure depicted the dendritic growth of the Al-V intermetallic phases represented by the grey colour (primary dendrite grains) with secondary arms (secondary dendrite grains) forming on both sides of the primary dendrite grains. Typical dendritic structures, characteristics of Al-based metals as dendrite microstructure, are found to form during casting and welding processes [29,30,31,32]. The phases identified in the SEM images are grey labelled as A (the $Al_3V$ and $Al_8V_5$ phases), light grey labelled as B (the $Al_{21}V_2$ phase) and dark grey labelled as C (the Al-rich phase) in Fig. 2b.

It has been reported that the microstructural features are cooling rate sensitive [33]. Therefore, due to the fast-cooling rate, only microstructural refinement of the dendritic structure was observed as well as globularization (Fig. 2b), but no significant improvement of their shapes as reported by others [34, 35].

Figure 3 shows the spatial distribution of the Al and V elements. The average composition of Al was found to be 63 wt. % and that of V 37 wt. % with a standard deviation of 5 and 4 wt. %, respectively. The elemental composition of the alloy of 62.9 Al and 37.1 wt. % V was found to be comparable to the theoretical 60Al-40V master alloy as well as the ICP analysis. The atomic ratio of the Al to V (Al: V) of the dominant phases with dendrite morphology was found to be approximatively 3:1, Fig. 3, and this is in agreement with what others have found [17, 31].

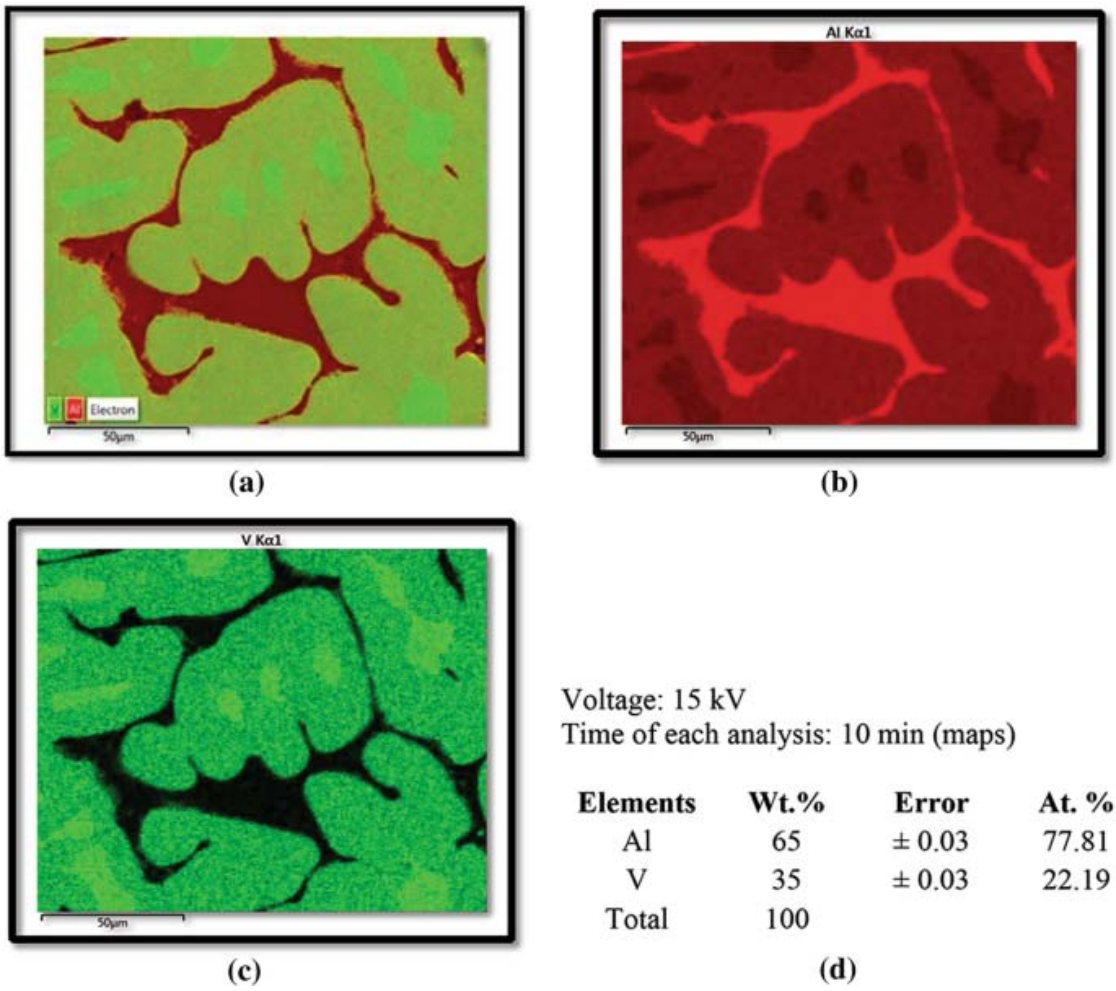


**Fig. 3.** SEM/EDS micrographs showing (**a**) elemental distribution, (**b**) Al, (**c**) V in the master alloy (**d**) the average elemental composition of the scanned area was 65 wt. % Al-35 wt. % V

Figure 4 shows SEM micrographs and EDS spectra of the alloy after DSC-TG tests at different temperatures. From the EDS analysis, based on the weight percentage of the dominant phases, the grey phase was identified to be V-rich, while the light and dark grey are Al-rich phases. The dominant phase labelled as A which is V-rich according to the analysis corresponds to the $Al_3V$ and $Al_8V_5$ phases. These phases are in agreement with the Al-V phase diagram by Thermo-Calc™ [28]. The light grey and dark grey phases were identified to be Al-rich phases (> 80 wt.% Al), with traces of V in solution such as the $Al_{21}V_2$ phase (8.7–15.9 wt.% V) that did not dissolve completely during the solution treatment. The presence of the $Al_{21}V_2$ phase which is occasionally found in as-cast alloys [29,30,31] is attributed to the increased Al content and cooling rate [29]. However, this phase could not be easily distinguished from the Al phase, under SEM as they have a very close chemical composition.

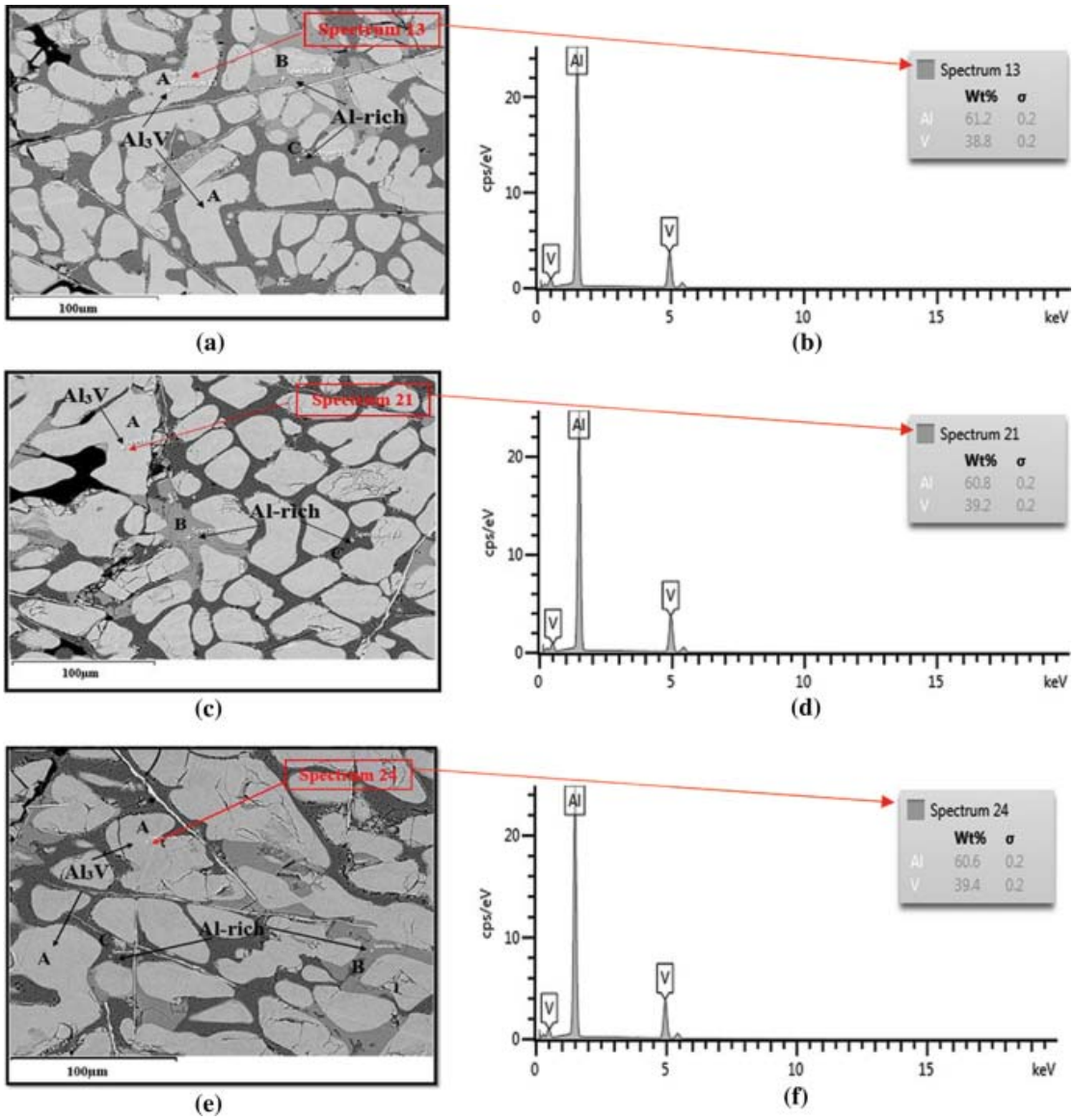


**Fig. 4.** SEM micrographs and EDS spectra analysis of the alloy after DSC-TG tests at (**a**)-(**b**) 1100, (**c**)-(**d**) 1300 and (**e**)-(**f**) 1400 °C, respectively

The results further confirmed the microstructural findings which reveal the stability of the three phases namely the grey, light grey and dark grey phases dominated by the Al and V elements. Table 2 presents the summary of the phases identified in the produced master alloy as well as the elemental chemical composition of the intermetallic phases after the DSC-TG analysis at the studied temperatures.

The phases in the alloy were principally identified to be $Al_3V$ phase and $Al_8V_5$ intermetallic compounds based on the weight percentage and according to the Al-V equilibrium binary phase diagram [28]. The volume fraction of the dominant $Al_3V$ phase on the different micrographs before and after heat treatment was determined through a combination of manual point count and thresholding methods in Image J® software©. These methods helped in the assessment and explanation of the microstructural evolution and stability of the phases after heat treatment between 1100 and 1400 °C.

**Table 2.** Summary of phases and elemental composition after the DSC-TG analysis

| Scanned region | Description | Chemical composition | | Phase |
|---|---|---|---|---|
| | | Al, wt.% | V, wt.% | |
| 1 | Grey | 61.2 | 38.8 | $Al_3V$+ $Al_8V_5$ |
| 2 | Light grey | 84.2 | 15.8 | Al-rich+$Al_{21}V_2$ |
| 3 | Dark grey | 98.7 | 1.3 | Al-rich |
| 4 | Grey | 60.8 | 39.2 | $Al_3V$+ $Al_8V_5$ |
| 5 | Light grey | 83.9 | 16.1 | Al-rich+$Al_{21}V_2$ |
| 6 | Dark grey | 89.9 | 10.1 | Al-rich+$Al_{21}V_2$ |
| 7 | Grey | 60.6 | 39.4 | $Al_3V$+ $Al_8V_5$ |
| 8 | Light grey | 84.6 | 15.4 | Al-rich+$Al_{21}V_2$ |
| 9 | Dark grey | 98.3 | 1.7 | Al-rich |

Figure 5 shows an illustration of the volume fraction estimation of the dominant $Al_3V$ phase. The volume fraction of the $Al_3V$ phase was determined to be between 78 and 81 % as shown in Fig. 6. As may be seen, there wasn't a significant change in the volume fraction of the phase which explains the stability of the $Al_3V$ phase during this temperature interval. This agrees with the Thermo-Calc™ predictions, as the $Al_3V$ phase was found to be the most stable phase in the Al-V system in the temperature range of 800–1400 °C [28].

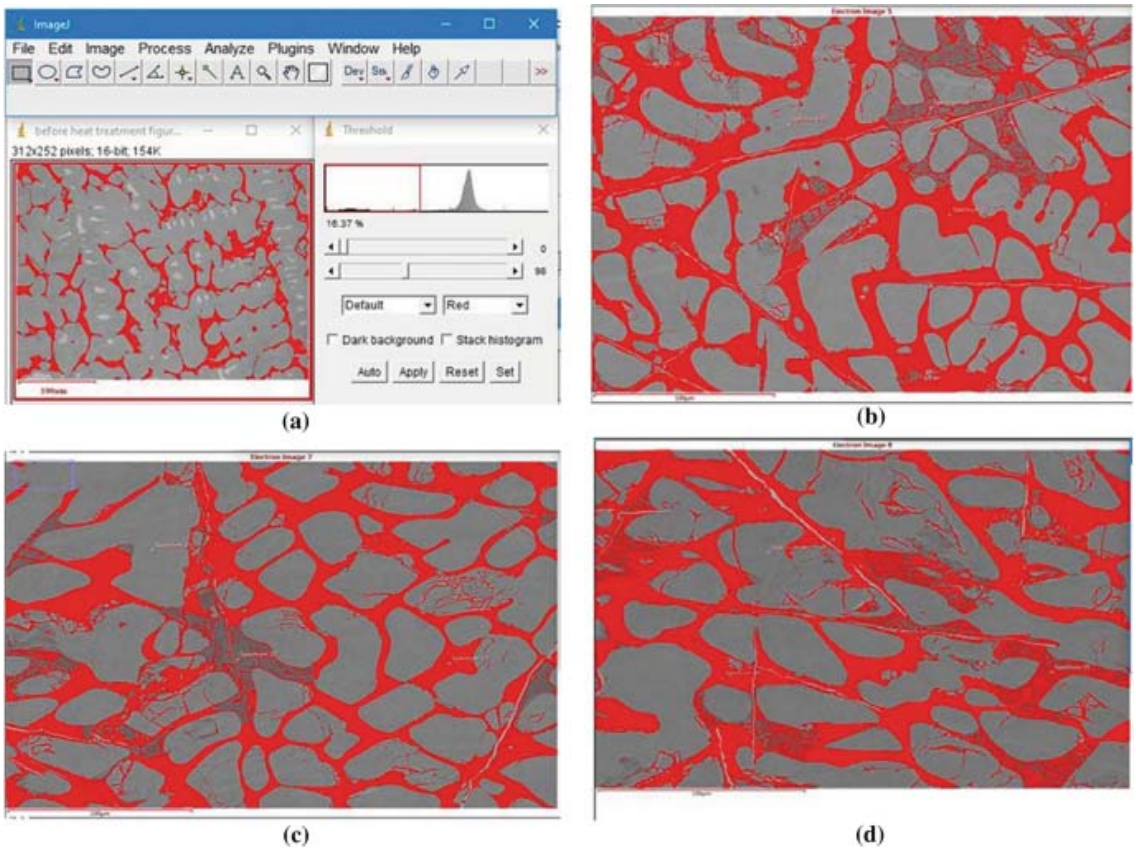


**Fig. 5.** An illustration of the volume fraction estimation of the $Al_3V$ phase through thresholding procedure using the Image J® software © (**a**) before and after DSC-TG tests at (**b**) 1100, (**c**) 1300, and (**d**) 1400 °C, respectively

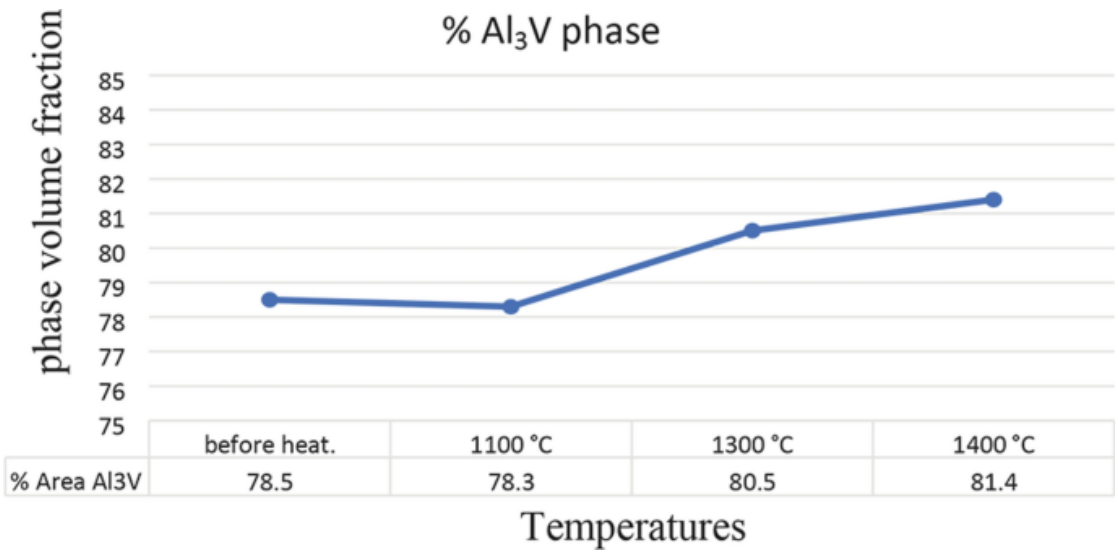


**Fig. 6.** Volume fraction of the $Al_3V$ phase as a function of temperature

***Phase Transformations and Crystal Structures of the Produced Master Alloy***

According to the Thermo-Calc™ predictions, the intermetallic compounds in the 60Al-40V master alloy included the $Al_8V_5$, $Al_3V$ and $Al_{23}V_4$ [28]. These and all the other intermetallic compounds were expected to dissolve at melting temperature [17]. Based on the Al-V equilibrium binary phase diagram [28] and crystal structure of the phases, the liquidus temperature of the Al-40 wt.% V alloy is about 1910 °C. At this temperature, the V dissolves into the molten aluminium completely. With the drop of temperature, the peritectic reaction $L+V \rightarrow Al_8V_5$ occurs at 1660 °C [17, 31]. This is followed by $V+ Al_8V_5 \rightarrow Al_3V$ at the temperature of 1360 °C and the transformation from $Al_3V$ to $Al_{23}V_4$ at the temperature of 735 °C [28, 36]. In this work, the $Al_8V_5$ transformed to the $Al_3V$ phase at a temperature of 1660 °C. Therefore, the $Al_3V$ phase was found to be the dominant and most stable phase due to the high Al content and cooling rate during solidification. However, due to the fast-cooling rate, there was not enough time for the transformation from the $Al_3V$ to the $Al_{23}V_4$ phase.

The XRD patterns of the produced 60Al-40V master alloy in the as-cast conditions and after reheating by the DSC-TG analysis are shown in Fig. 7.

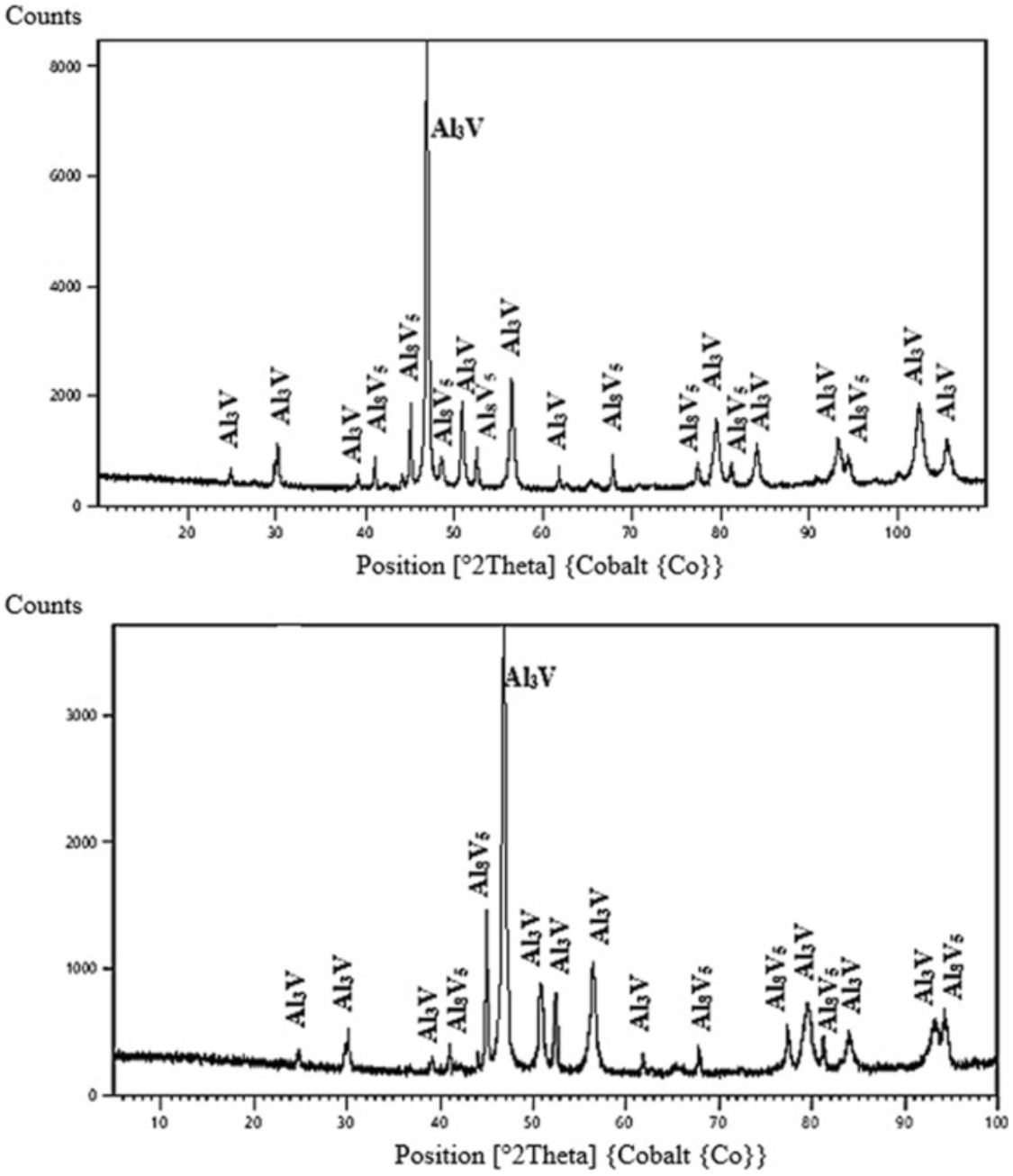


**Fig. 7.** XRD patterns showing the phases of (**a**) the starting material of the 60Al-40V master alloy and (**b**) after DSC-TG analysis

The XRD patterns revealed the presence of high-intensity diffraction peaks of $Al_3V$ and $Al_8V_5$ intermetallic phases principally. Minor peaks can sometimes be lost in the background noise and, therefore, are not detectable [37]. Therefore, the Al-fcc phase or other Al-rich phases such as the $Al_{21}V_2$ and $Al_{23}V_4$ characterized by peaks of lesser intensity could not be detected in the XRD patterns, but the presence of the high crystalline structure such as the $Al_3V$ and $Al_8V_5$ with high-intensity peaks was observed. Their structures were analysed to be cubic ($Al_3V$) (I4/mmm tL8) and cubic $Al_8V_5$ (I-43m cl2) as illustrated in the ICDD data [38] which indicated that the system was not amorphous but crystalline. Therefore, the dominant phases which were detected before and after DSC-TG analysis were the $Al_3V$ and the $Al_8V_5$ intermetallic phases

(Fig. 7). In other words, the stable phases detected by XRD analysis agreed well with the Thermo-Calc$^{TM}$ predictions [28] and the results of EDS analysis.

### *Thermal Analysis—Simultaneous DSC-TG*

Figure 8 shows the DSC-TG curves illustrating the transition temperatures occurring in the material for the temperatures of 1100, 1300 and 1400 °C, respectively. It can be observed that phase transformations occurred at specific points in the temperature-phase transformations curves for both the first and the second heating–cooling cycles.

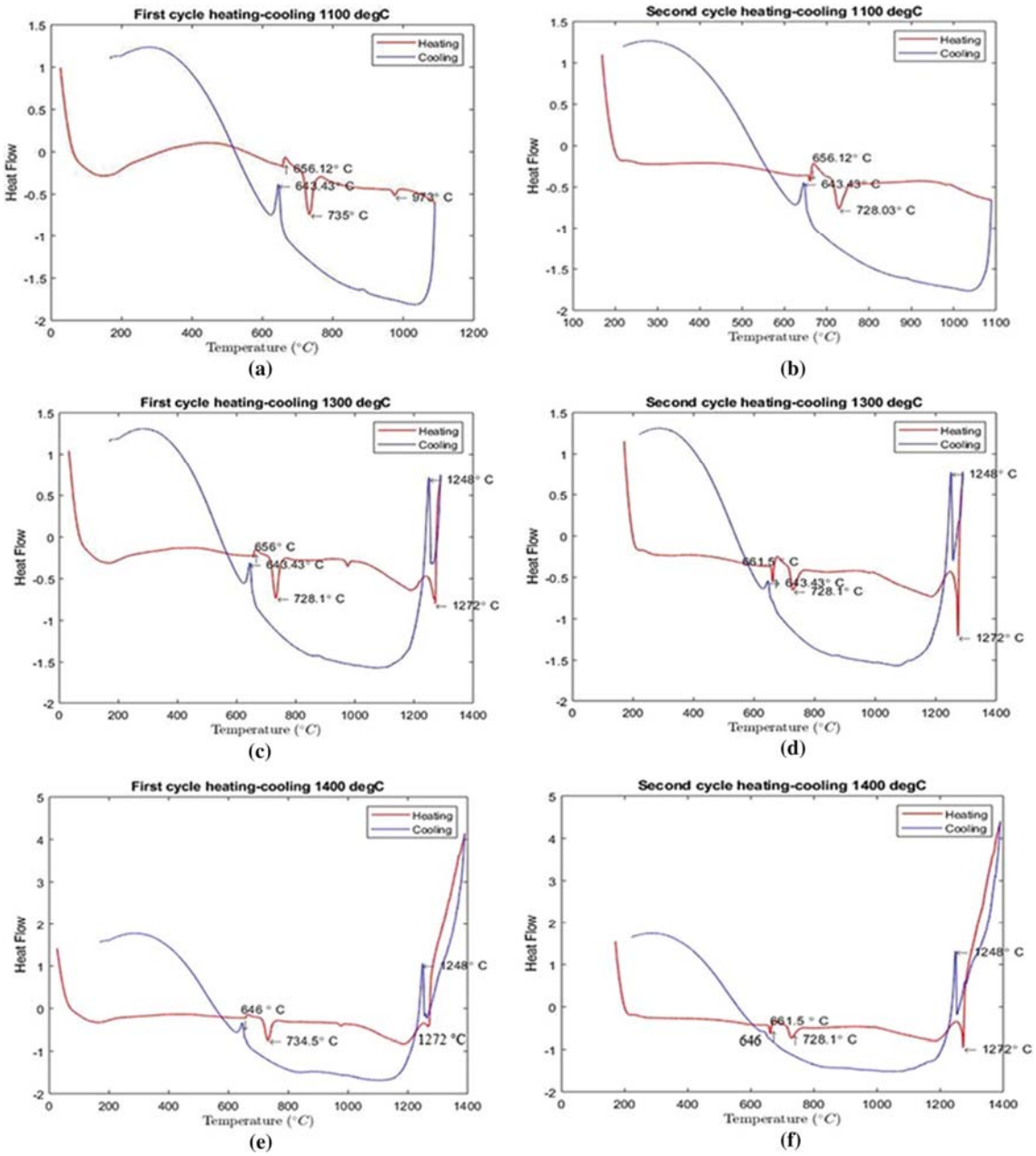


**Fig. 8.** The heat flow curves during DSC-TG tests for (**a**) first heating–cooling cycle at 1100 °C, (**b**) second heating–cooling cycle at 1100 °C, (**c**) first heating–cooling cycle at 1300 °C, (**d**) second heating–cooling cycle at 1300 °C, (**e**) first heating–cooling cycle at 1400 °C, (**f**) second heating–cooling cycle at 1400 °C

The high intensities of high-temperature transformations in the DSC-TG curves corresponded to the invariant reactions of $L+Al_8V_5 \rightarrow Al_3V$ (at 1272 °C) and $L+Al_3V \rightarrow Al_{23}V_4$ (at 728 °C). It can be observed that the peaks correspond with the invariant reactions as obtained by Richter [39], especially for the invariant reaction $L+Al_8V_5 \rightarrow Al_3V$ (at 1270 °C) and the invariant reaction $L+Al_3V \rightarrow Al_{23}V_4$ (at 736 °C). The peak observed at a temperature of 643 °C corresponded to the presence of the Al-fcc with traces of V in solution (the $Al_{21}V_2$ which did not dissolve completely) as predicted by Themo-Calc™ (at 664 °C). The obtained reactions were cooling rate and Al- content dependent. Unlike the XRD, all three-phase transformations were observed during the DSC-TG analysis, and as expected for non-equilibrium cooling rates, all the transformation temperatures were found to be lower than predicted by Thermo-Calc™ [28]. In brief, the stability of the $Al_3V$ phase before and after DSC-TG analysis was fairly well-established using EDS and was confirmed by XRD with only a small amount of the $Al_8V_5$ phase. The volume fraction of the $Al_3V$ dominant phase was estimated to be about 80% and was evenly distributed in the specimen demonstrating the homogeneity of the microstructure produced through the aluminothermic process.

## Conclusion

The 60Al-40V master alloy produced by the aluminothermic reaction process was investigated through different techniques, and the following conclusions were drawn:

- A master alloy with an average composition of 63 Al -37wt. %V was produced by the aluminothermic reaction process;
- The predominant stable phases were found to be the $Al_3V$ and $Al_8V_5$.
- The amount of $Al_8V_5$ phase formed was found to decrease with decreasing temperature and decreasing V content, while the converse was found to be true for the $Al_3V$.
- The volume fraction of the dominant $Al_3V$ phase was estimated to be about 80% before and after heat treatment and was evenly distributed in the specimen demonstrating both the homogeneity and stability of the microstructures produced through the aluminothermic process for a given homogenization temperature.
- However, the $Al_3V$ phase was found to increase slightly with an increase in the homogenization temperature.

## Acknowledgements

The authors are grateful to the South African Council for Scientific and Industrial Research (CSIR) for the provision of materials and the University of Pretoria for the provision of equipment and the financial support.

## References

1. B. Lindahl, X.L. Liu, Z.K. Liu, M. Selleby, A thermodynamic re-assessment of Al-V toward an assessment of the ternary Al-Ti-V system. Calphad Comput. Coupling Phase Diagr. Thermochem. **51**, 75–88 (2015)
2. A. Kostov, D. Zivkovi, Thermodynamic analysis of alloys Ti-Al, Ti – V, Al – V and Ti-Al – V ˇ. J. Alloy. Comp. **460**, 164–171 (2008)
3. D. Carou, E.M. Rubio, B. Agustina, M.M. Marín, Experimental study for the effective and sustainable repair and maintenance of bars made of Ti-6Al-4V alloy. Application to the aeronautic industry. J. Clean. Prod. **164**, 465–475 (2017). https://doi.org/10.1016/j.jclepro.2017.06.095

4. Peters M, Leyens C. (2003) Titanium and titanium alloys: fundamentals and applications. In: Christoph Leyens, Manfred Peters. (Eds.), Wiley, 1: 513
5. R.R. Boyer, An overview of the use of titanium in the aerospace industry. Mater. Sci. Eng. A. **213**(1–2), 103–114 (1996)
6. I. Inagaki, T. Takechi, Y. Shirai, N. Ariyasu, Application, and features of titanium for the aerospace industry. Nippon Steel Sumitomo Met Tech. **106**(106), 22–27 (2014)
7. M. Niinomi, Mechanical biocompatibilities of titanium alloys for biomedical applications. J. Mech. Behav. Biomed. Mater. **1**(1), 30–42 (2008)
8. H.J. Rack, J.I. Qazi, Titanium alloys for biomedical applications. Mater Sci Eng C. **26**, 1269–1277 (2006)
9. German RM. (1996) German, Sintering theory and practice. Chapiter
10. J. Capus, Conventional PM is still a challenge for titanium and alloys. Met. Powder. Rep. **69**(6), 18–20 (2014). https://doi.org/10.1016/S00260657(14)70274-7
11. Y.Z. Qui, Y. Grjotheim, K. Kvande, Formation of Al-Mn master alloys by thermal reduction and by electrolysis of manganese dioxide in cryolite-alumina melts. Aluminium. **64**(2), 603–605 (1988)
12. Q. Zhuxian, Z. Zhonglin, K. Grjotheim, H. Kvande, Formation of Al-Si alloys by electrolysis and by thermal reduction of silica in cryolite-alumina melts. Aluminium. **63**, 1247–1250 (1987)
13. Z. Qui, M. Zhang, Y. Yue, Z. Che, K. Grjotheim, H. Kvande, Formation of aluminium-titanium alloys by electrolysis and by thermal reduction of titania in cryolite-alumina melts. Aluminium. **4**(6), 606–609 (1988)
14. C.C. Koch, Intermetallic matrix composites prepared by mechanical alloying - A review. Mater. Sci. Eng A. **244**, 39–48 (1998)
15. C. Nishimura, C.T. Liu, Reaction sintering of Ni3Al to near full density. Scr. Metall. Mater. **26**, 381–385 (1992)
16. R. Hahn, H. Andorfer, H.J. Retelsdorf, Production of master alloys for the Titanium Industry by the GfE-Two-stage-process. Metall. **39**(2), 126–127 (1985)
17. H. Wan, B. Xu, L. Li, B. Yang, D. Li, Y. Dai, A novel method of fabricating Al-V intermetallic alloy through electrode heating. Metals (Basel). **9**(5), 558 (2019)
18. Y.M. Gorji, M. Soltanieh, A. Habibolahzadeh, Production of Al-Si master alloy by aluminothermic reduction of silica in molten cryolite. Can. Metall. Q. **46**(4), 385–390 (2007)
19. M. Hosseinpouri, S.A. Mirmonsef, M. Soltanieh, Production of Al-Ti master alloy by aluminothermic reduction technique. Can. Metall. Q. **46**(2), 139–144 (2007)
20. E. Gock, B. Friedrich, Aluminothermic production of titanium alloys (PART 2): impact of activated rutile on process sustainability. Metallur. Mater Eng. **21**(2), 101–114 (2015)
21. A.N.M. Omran, Fabrication and characterization of Al-based in situ composites reinforced by Al3V intermetallic compounds. Mater. Sci. Technol. Conf. Exhib. **2**(2), 1389–1400 (2013)
22. L.L. Wang, Z.A. Munir, Y.M. Maximov, Thermite reactions: their utilization in the synthesis and processing of materials. J. Mater. Sci. **28**, 3693–3708 (1993)
23. G. Sauthoff, Intermetallics, in *Materials Science and Technology*. ed. by R.W. Cahn, P. Haasen, E.J. Kramer (Wiley-VCH Verlag, Germany, 2007)
24. C.T. Liu, J. Stringer, J.N. Mundy, L.L. Horton, P. Angelini, Ordered intermetallic alloys: an assessment. Intermetallics. **5**, 579–596 (1997)
25. C.T. Liu, J.O. Stiegler, Ductile ordered intermetallic alloys. Science. **226**, 636–642 (1984)

26. M.R. Parsa, M. Soltanieh, On the formation of Al3Ni2 intermetallic compound by aluminothermic reduction of nickel oxide. Mater. Charact. **62**(7), 691–696 (2011). https://doi.org/10.1016/j.matchar.2011.04.013
27. Akerkar DD. (1994) Physico Chemical aspects of alumino-thermic reduction in the production of Low carbon Ferro-Alloys by. In: 4th Refresher Course on Ferro Alloys
28. T.O. Mapoli, K.A. Annan, C.W. Siyasiya, K. Mutombo, Preparation and microstructural characterization of the 60Al-40V master alloy. IOP Conf Ser Mater Sci Eng. **655**(1), 1–8 (2019)
29. J. Lai, C. Shi, X.G. Chen, Effect of V addition on recrystallization resistance of 4150 aluminium alloy after simulative hot deformation. Mater. Charact. **96**, 126–134 (2014). https://doi.org/10.1016/j.matchar.2014.07.28
30. O. Carlson, D. Kennedy HW. (1955) The aluminium-vanadium alloy system. Am Soc Met. 47:520–37
31. Q.F. Zhu, Y. Meng, Y.L. Kang, S.P. Kong, Y.P. Ou, Y.B. Zuo, Effect of cooling rate on morphology and type of vanadium-containing phases in Al-10V master alloy. China. Foundry. **16**(5), 300–306 (2019)
32. P. Snopiński, M. Król, T. Tański, B. Krupińska, Effect of cooling rate on microstructural development in alloy ALMG9. J. Therm. Anal. Calorim. **133**(1), 379–390 (2018)
33. A. Das, S. Sunil, R. Kapoor, Effect of cooling rate on the microstructure of a pressure vessel steel. Metallogr. Microstruct. Anal. **6**, 795–805 (2019). https://doi.org/10.1007/s13632-019-00585-6
34. N. Haghdadi, A.B. Phillion, D.M. Maijer, Microstructure characterization and thermal analysis of aluminium alloy B206 during solidification. Metallur. Mater. Trans. A. **46**(5), 2073–2081 (2015)
35. B. Benjunior, A.H. Ahmad, M.M. Rashidi, M.S. Reza, Effect of different cooling rates condition on thermal profile and microstructure of aluminium 6061. Procedia Eng. **184**, 298–305 (2017). https://doi.org/10.1016/j.proeng.2017.04.098
36. H. Okamoto, Al-V (Aluminum-Vanadium). J. Phase Equilib. Diffus. **33**, 491 (2012)
37. Speakman SA, Ph D. Introduction to X-Ray Powder Diffraction Data Analysis an X-ray diffraction pattern is a plot of the intensity of X-rays scattered at different angles by a sample
38. M. Hellenbrandt, The inorganic crystal structure database (ICSD) - Present and future. Crystall Rev. **10**, 17–22 (2004)
39. K.W. Richter, H. Ipser, Al-V phase diagram between 0 and 50 atomic percent vanadium. Zeitschrift fuer Met Res Adv Tech. **91**(5), 383–388 (2000)